Chinese Science Bulletin 2006 Vol. 51 No. 11 1355—1367

DOI: 10.1007/s11434-006-1355-2

Large-scale low-frequency rainfall regimes and their transition modes in summertime over China

REN Hongli[1,2], ZHANG Peiqun[2], CHOU Jifan[1], LI Weijing[2] & GAO Li[3]

1. College of Atmospheric Sciences, Lanzhou University, Lanzhou 730000, China;
2. Laboratory for Climate Studies, National Climate Centre, China Meteorological Administration, Beijing 100081, China;
3. LASG, Institute of Atmospheric Physics, Chinese Academy of Sciences, Beijing 100029, China

Correspondence should be addressed to Zhang Peiqun (email: zhangpq@cma.gov.cn)

Received September 24, 2004; accepted August 4, 2005

Abstract Seven large-scale low-frequency rainfall regimes (LFRRs) in summertime are identified for China in a 10-dimensional phase space by using a 40-year daily precipitation dataset. Corresponding to the local extrema of observed probability density in phase space, the LFRRs are characterized by the persistence and transitions that reflect the spread and jump features of low-frequency rainfall centers. The LFRRs are generally consistent with summer monsoon rainbelts on the intraseasonal timescale, and there exist the preferred transition relationships between the LFRRs. Four LFRRs' transition modes (LFRRTMs), which are the dominant components of the interannual and intraseasonal variability of summer rainfall in China, are further induced. Analyses of atmospheric circulation system show that the anomalies of the subtropical high over the western Pacific (SHWP) and blockings in mid-high latitudes, the low-latitude circulation anomalies, and the wavetrains over the East Asia-Pacific region (EAPWs), play crucial roles in the occurrence and transitions of the LFRRs. Moreover, the evolution of the SHWP and blockings, the distribution and movement of the EAPWs, and the intraseasonal variability of the East Asian-Pacific jet stream may be principal factors of the formations of the LFRRTMs.

Keywords: summer rainfall, low-frequency rainfall regime, phase space, transition.

It is well known that the predictable period of daily weather is generally within 2—3 weeks, so spatio-temporal mean predictands have to be employed in the monthly, seasonal, and annual predictions. At present, rainfall patterns (RPs)[1−5] are the key forecasting objects for summer in China[5,6]. These patterns are usually classified by the departures of total precipitation from climatological means in flood seasons. However, their application in operational forecast is not satisfactory in terms of significance in the correlations between the RPs and previous predictors[6,7]. For example, the anomalous atmospheric circulation and earlier signals are obviously different between 1998 and 1999 although the two years possess similar patterns of summer rainfall anomalies and both belong to the south pattern[8]. Because there usually exist several large-scale low-frequency rainfall (LFR) processes during summer, it is unclear at present whether the impact of anomalous previous predictors is on the seasonal mean rainfall or on the intraseasonal large-scale LFR process. Thus, it is necessary to know forecasting objects again.

Evolution of circulation beyond predictability period is not completely chaotic, which is clearly reflected by the persistence and recurrence of certain weather regimes in specific geographical locations[9]. Similar situations also exist in the rainfall dominantly influenced by circulation. Many studies have documented that summer rainfall in China exhibits significant intraseasonal low-frequency variations and spatial spread features[10−13], and LFR is an important component in summer rainfall[14,15]. It is found from operational experience of climate prediction that large-scale LFR usually affects persistently some region at a time but another region at a different time. Such persistence and transitions of the distribution of intraseasonal LFR anomalies often appear as different spatial regimes that are defined as large-scale low-frequency rainfall regimes (LFRRs), or rainfall regimes (RRs) for short. Thus, it can be seen that total precipitation anomalies in flood season are actually the statistical mean of some LFRRs. Consequently, it will be helpful for searching objective forecasting objects to reveal the features of persistence and transitions of the LFRRs, circulation backgrounds, and the main impact factors, which is a new worthy approach for flood-season rainfall forecasting.

If the observed persistently precipitation can be expressed as state points, the main gathering regions of the state points, representing large-scale RRs, can be formed in phase space in the process of long-term evolutions of rainfall, as demonstrated from the prelimi-

nary studies[16,17]. Furthermore, the low-frequency variability of atmospheric circulation is characterized by planetary flow regimes (PFRs). Correspondingly, in phase space, the state points edge away for a period of time within any PFR, and thereafter transfer into another PFR. Such persistence and transitions of the PFRs show the primary characteristics of spatio-temporal evolution of the large-scale low-frequency circulation[18]. Hence, to depict the features of spatio-temporal variations of LFR, we will first identify the LFRRs by introducing a method[19] that can detect the local extrema of observed probability density in phase space, and then examine the possible preferred transition (PT) relationships between them, and discuss the physical mechanism for the LFRRs, their transitions, and circulation anomalies.

1 Data and methodology

The precipitation data used in the present study are the daily observations of 742 stations (Fig. 1(a)) from the National Meteorological Information Center of China Meteorological Administration. Considered the influences of the inhomogeneous distributions and poor representativeness of only one hundred stations or more in the preliminary studies[16,17], an interpolation from observation into 2°×2° grids over China (Fig. 1(b)) is carried out by employing the Cressman's procedure[20], and a new daily grid precipitation dataset over 40 years starting from January 1962 to December 2001 is obtained. The regions including the Qinghai-Tibet Plateau and northern desert, where there are few stations or short gauges, are eliminated. Thus, 200 grid points are utilized for this paper. Since the interpolation used above is like a spatial smoothing operator, the information of large-scale precipitation is emphasized by filtering out the disturbances of meso- and submeso-scales.

By using the 40-year end-to-end grid data from 1 May through 30 September for each year, the seasonal cycle averaged over 40 years is removed from the daily gridpoint precipitation to define the precipitation anomalies (UNF hereafter) with 6120 samples. To focus on the large-scale low-frequency rainfall component, we apply a 20-day low-pass Gaussian filter to the UNF data and attain new anomalies, which are referred to as LF20. Samples outside the annual 153-day period were used in this filtering so that those within the period were appropriately filtered without boundary influences. Furthermore, the standardized gridpoint data

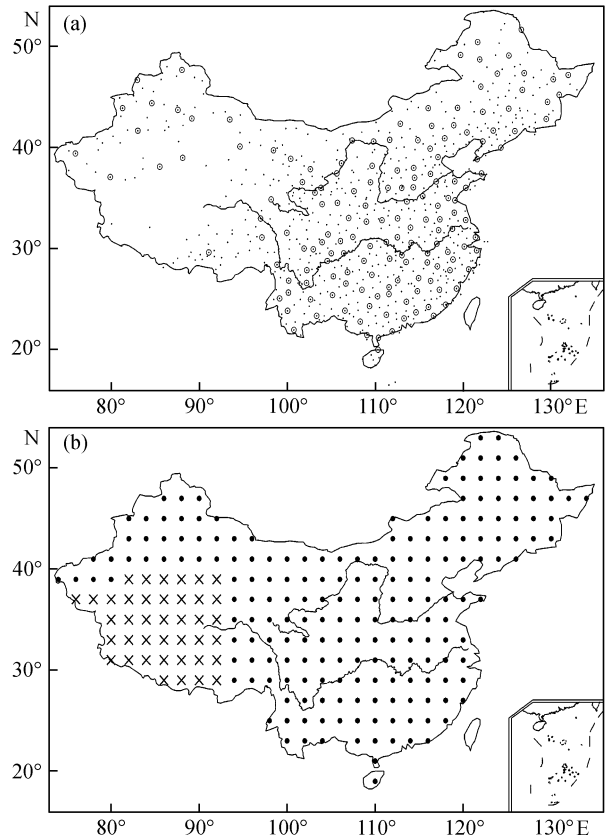

Fig. 1. Distributions of the stations (a) and interpolated grids (b) over China. (a) Dots stand for the 742 stations and circles for the 160 base stations; (b) dots stand for the 200 grids and crosses for the eliminative grids.

will be used for latter operations. The daily data fields from the NCEP/NCAR reanalysis (unfiltered), including 500-hPa heights, 850-hPa winds, and 200-hPa zonal winds, will be also utilized for circulation analysis.

In order to extract information of primary modes of precipitation anomalies in 200-dimensional phase space, where 200 grid points exist, it is necessary to reduce the dimensionality of the data. It has been widely documented that the EOF analysis can be employed to determine a few degrees of freedom spanning low-dimensional attractors[21], which is an effective technique to achieve the above purpose. As an intercomparsion, the EOF decomposition is applied to standardizing the UNF and LF20 data, as well as the simultaneous unfiltered daily anomalies of the 160 base stations over China (denoted as UNF160, see Fig. 1(a)), respectively (Table 1). As a whole, the EOFs' percentage variances (PVs) associated with the three kinds of datasets decrease slowly from the first mode to the latter, respectively, and no single mode is dominant, reflecting the

Table 1 Percentage variances (PVs) and cumulate percentage variances (CPVs) associated with three dataset EOFs (%)

EOF	UNF160		UNF		LF20		EOF	UNF160		UNF		LF20	
	PV	CPV	PV	CPV	PV	CPV		PV	CPV	PV	CPV	PV	CPV
1	4.35	4.35	6.25	6.25	10.27	10.27	10	1.57	25.84	2.49	37.16	2.60	50.69
2	3.63	7.99	4.73	10.99	7.05	17.32	11	1.44	27.28	2.21	39.37	2.19	52.88
3	3.15	11.14	4.40	15.38	6.21	23.53	12	1.43	28.71	1.93	41.31	2.11	54.99
4	2.83	13.97	3.89	19.27	5.76	29.28	13	1.39	30.10	1.87	43.17	1.86	56.85
5	2.34	16.31	3.81	23.08	4.89	34.17	14	1.35	31.46	1.80	44.97	1.77	58.61
6	2.21	18.52	3.44	26.52	3.92	38.09	15	1.25	32.70	1.74	46.71	1.69	60.30
7	2.12	20.64	2.90	29.42	3.55	41.64	20	1.00	38.32	1.33	54.16	1.13	67.05
8	1.90	22.54	2.70	32.13	3.49	45.13	25	0.86	42.94	1.12	60.12	0.90	72.12
9	1.73	24.27	2.55	34.67	2.96	48.09	30	0.78	46.98	0.89	65.00	0.71	76.03

complexity of daily precipitation anomalies. The PVs interpreted by the principal EOFs of grid data, furthermore, obviously increase in virtue of the smoothing effect of the spatial interpolation, compared with those of station data. It can also be seen that the PVs contributed by the principal EOFs of the LF20 data are higher than those of the unfiltered data because only the prolonged low-frequency information is held. Usually, the EOF analysis is sensitive to spatial domain of data, but the EOFs introduced as the orthogonal bases for reducing the degree of freedom are stable[22]. Thus, the EOF analysis is only used to span the phase space in the current paper[16,17,19,21,23] in order to extract the principal information of LFR variability, whereas the actual situation of a certain EOF is not especially considered.

2 Identification of the LFRRs

Since the distributions of state points are inhomogeneous, it seems that the LFRRs may be directly identified if probability density functions (PDFs) in the phase space could be precisely calculated. However, depending on all of the existing available samples, the PDFs of more than 3 dimensions cannot be exactly estimated[16,17]. According to Table 1, it is necessary to have at least 10 EOFs for objective classifications with appropriate 50% PVs. Therefore, a cluster analysis method[19] is employed for classifications in terms of "distance" between state points in multi-dimensional phase space[17,19].

2.1 Clustering in phase space

In the process of clustering, the observed samples dominated by the leading EOFs are expected to utilize, which represent more information of large-scale anomalies, whereas those governed by the EOFs with minor PVs should be removed. Therefore, for every sample, we examine the signal-noise (S/N) ratio between the variance of the first m principal components (physical "signal") and that of the rest ("noise"), where m is unknown. The samples, the corresponding S/N ratio of which is greater than 1, will be used in the analysis. According to Table 1, as the cumulate PV of the first 12 EOFs reaches to about 55 percent, m is taken as 12 here. So, 3697 samples are ultimately chosen.

With the 3697 samples used, the cluster analysis is carried out in the phase space spanned by the first 10 EOFs that account for about 50 percent of the total variances. As seen in Table 1, the statistical separation between the PVs associated with the 10th and 11th EOF is also considered. The correlation coefficient p between state vectors in phase space is chosen as the clustering index of the cluster analysis. Clustering criteria prescribed here are that p between state points belonging to the same cluster is greater than r_1, and p corresponding to different clusters is smaller than r_2. In order to get the stablest RRs, by adjusting r_1 and r_2[17], seven principal clusters in the 10-dimensional space, namely the LFRRs that are in turn denoted as R_1—R_7, respectively, are determined under the condition of $r_1 = 0.65$ and $r_2 = 0.22$. Table 2 presents the clustering information of the seven LFRRs.

It can be seen from Table 2 that the number of samples falling into the LFRRs is more than one third of the total, and each RR occurs once or twice in every year with average duration (defined as the days covered by a RR event, where the event is defined as the days from the beginning to the ending of RR) being close to 6 days, which is quite long for large-scale rainfall anomalies. Considering the interval (defined as the days from the ending of certain RR to the beginning of next RR), the average duration-interval period of RRs is approximately 14 days. The events which last for 5 days are the most. Moreover, we also see that the num-

Table 2 Information of the LFRRs identified in 10-dimensional phase space of the LF20

LFRRs	Sample number	Event number	Number of events with given duration days										Average duration	Maximum duration	Average interval
			1	2	3	4	5	6	7	8	9	⩾10			
R_1	479	69	3	6	7	3	11	6	9	8	4	12	6.94	25	8.52
R_2	474	79	6	6	10	4	13	11	7	5	4	13	6.00	17	10.18
R_3	311	56	4	9	7	5	9	3	3	8	4	4	5.55	23	8.09
R_4	367	59	2	9	4	5	10	6	5	4	1	13	6.22	16	8.92
R_5	285	54	7	3	8	7	8	1	9	3	2	6	5.28	14	6.57
R_6	297	52	3	6	8	7	5	8	2	2	2	9	5.71	20	8.60
R_7	270	49	7	7	2	9	8	0	4	5	1	6	5.51	23	6.14
Sum	2483	418	32	46	46	40	64	35	39	35	18	63	Average 5.89	19.71	8.15

ber of the events whose duration is no less than 5 days exceeds half of the total, and the persistent events that last for more than 10 days, which may correspond to the large-scale rainfall anomalies associated with famous drought or flooding events in history, account for a considerable proportion of the total.

2.2 LFRRs' composites and corresponding circulation backgrounds

In physical space, the composite maps of seven LFRRs, as shown in Fig. 2, are obtained by arithmetically averaging their samples, respectively. Simultaneously, the composites of 850-mb wind anomalies and 500-mb height anomalies, as well as 200-mb zonal wind (Fig. 3 C_1—C_7), are also provided to examine the circulation background of every RR, where the composites of 200-mb zonal wind will be discussed in section 4.

(i) R_1: South of the Yangtze River (hereafter SY) regime (Fig. 2(a)). The features of the SY regime are similar to those of the conventional south pattern[5]. A dominant center of positive anomalies lies to the south of the Yangtze River and relatively weak negative anomalies are in most of the north. The corresponding circulation anomalies (Fig. $3C_1$) are characterized by a south-north "+ – +" wavetrain in the region of East Asia, where a significant center of negative anomalies exists in the mid-latitude areas of East Asia and the broad-area positive anomalies exist in the low-latitude ocean. Furthermore, anomalous circulation is also represented by the strong meridional pattern, such as the southward extension of the subtropical high in the western Pacific (hereafter SHWP), and the strong blocking in Northeast Asia, and the weaker southwest monsoon flows as a result of the positive anomalies from the northern India to the Bay of Bengal, which all together make the summer monsoon rainbelt in East Asia evidently southward.

(ii) R_2: Rainless regime (Fig. 2(b)). This regime, which often appears during the decay period of summer monsoon or the heavy drought years in history, is characterized by the significant negative anomalies over most of China except a southwest positive corner[17]. A countrywide rainless pattern was introduced by Wang *et al*.[4] to investigate summer rainfall anomalies in eastern China, which needs to be subjectively identified. In anomalous circulation fields, as shown in Fig. $3C_2$, there exists not only a deepened signal of the Aleutian Low, but also the northwest-southeast "– + –" wavetrain in the East Asian areas, which includes a dominant center of positive anomalies situated over Mongolia and its adjacent areas, and two centers of negative anomalies located in northern Siberia and over the Donghai Sea, respectively. In this condition, the whole China lies behind eastward East Asian trough, where westerly winds prevail and anomalous wind convergences are nearly inexistent.

(iii) R_3: Eastern regime. As seen in Fig. 2(c), one dominant positive center covers over the whole Northeast China, and the other positive anomalies exist in the regions from eastern North China through the mid-low Yangtze River valley (MLYRV), and the negative ones lie in the mid-western areas, which are similar to the northeastern regime[17], whereas the Northeast-North China pattern[4] has positive anomalies center in southern Northeast China. Anomalous circulation (Fig. $3C_3$) is mainly characterized by the multipole over the areas from East Asia to northwestern Pacific, and the "+ – + –" wavetrain from South China to northern Alaska, where there are the blockings in Middle Asia and Northeast Asia, and significant negative centers in northern North China and northwestern Pacific. Evidently, this configuration of anomalous circulation helps to cold and warm flows converging over Northeast China and the MLYRV, respectively. Moreover, the eastern regime seems to indicate the preference that

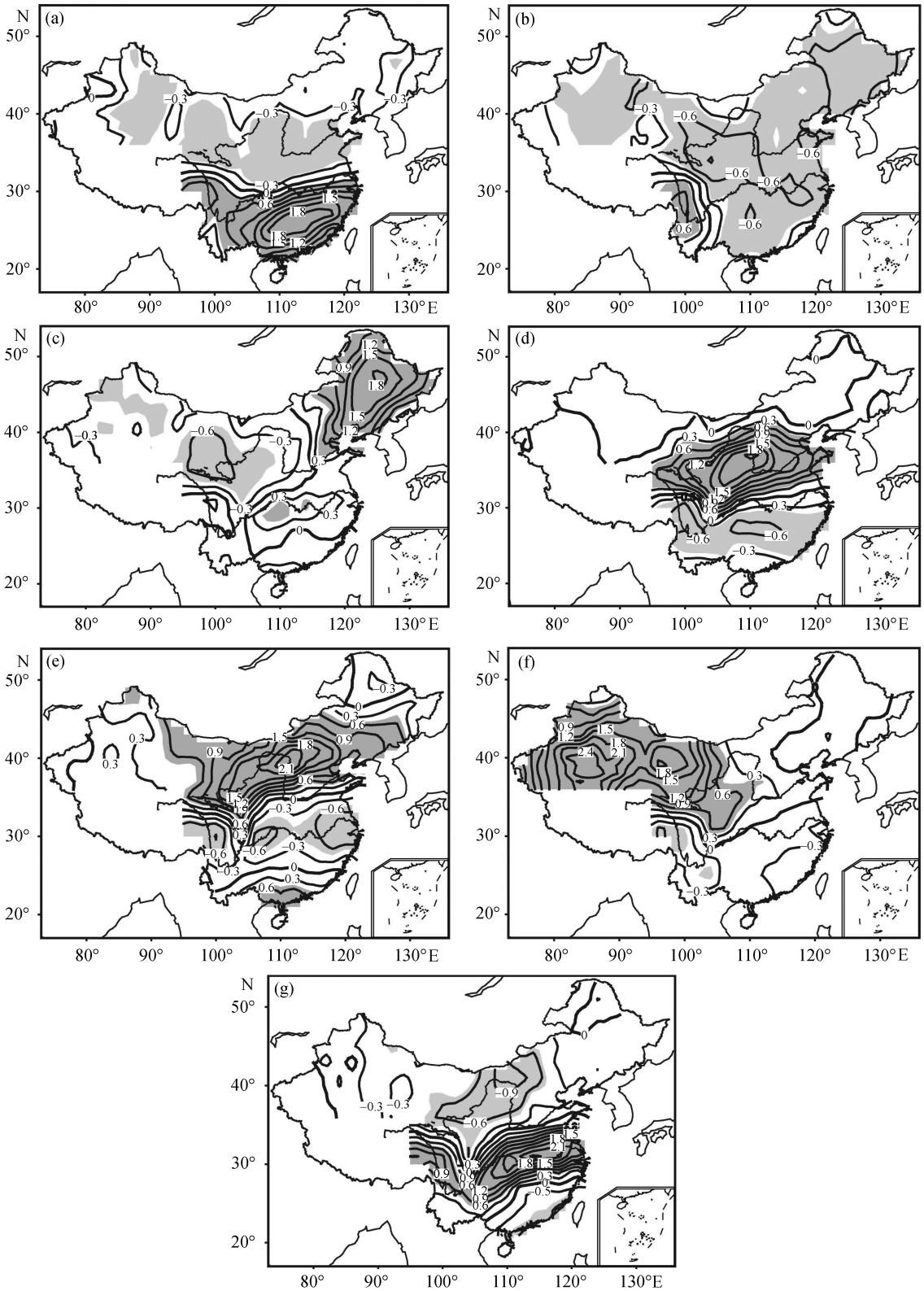

Fig. 2. Composite maps of the seven LFRRs. (a) R_1: SY regime; (b) R_2: rainless regime; (c) R_3: eastern regime; (d) R_4: YR regime; (e) R_5: northern regime; (f) R_6: northwestern regime; (g) R_7: YH regime. The areas over the 99% confidence level of *u*-test are shaded; Interval of contours is 0.3.

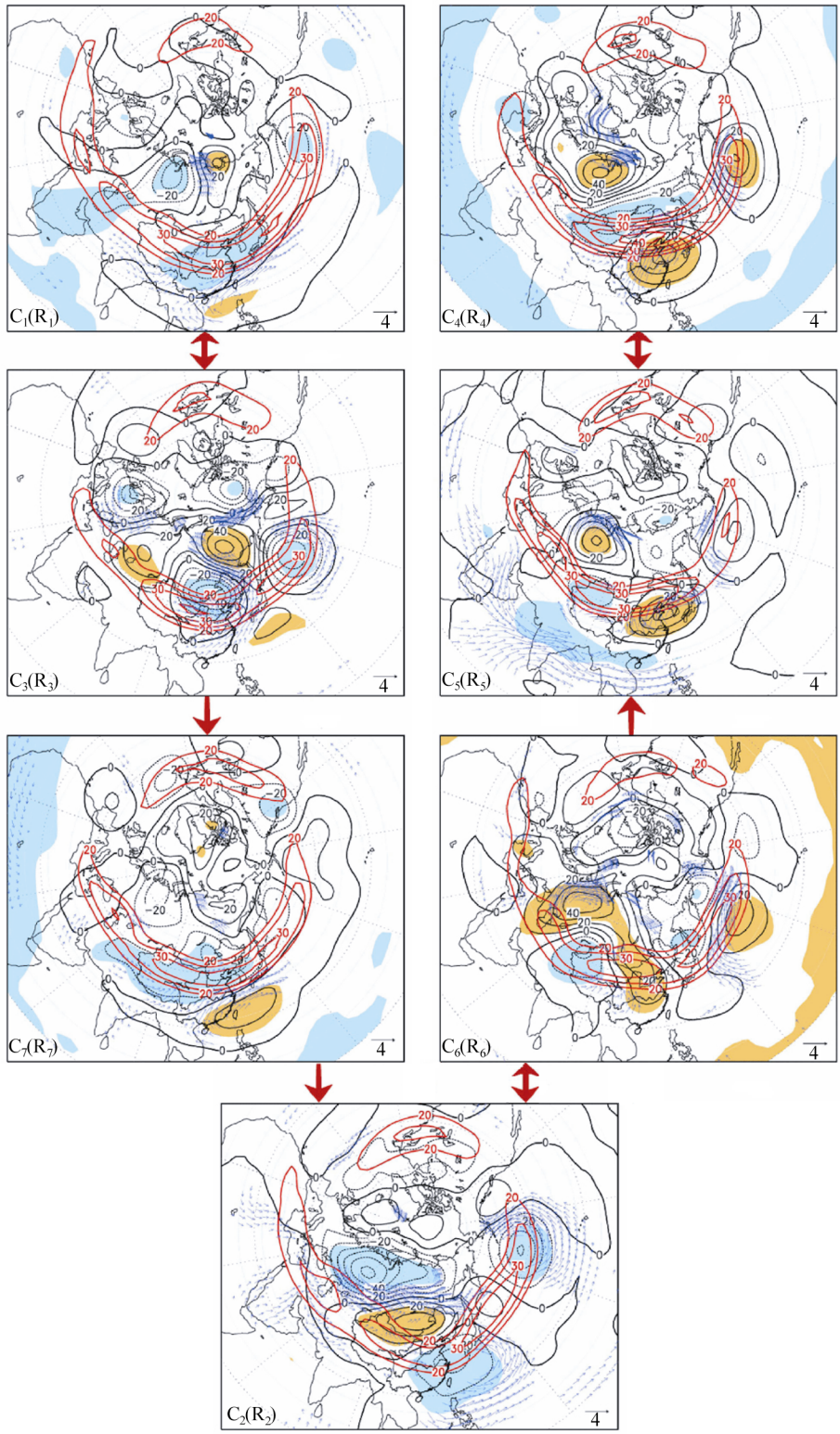

Fig. 3. Composite maps (C_1-C_7) of simultaneous circulation fields corresponding to the seven LFRRs (R_1-R_7). Black contours with 10gpm interval denote the 500-mb height anomalies and the areas over the 99% confidence level of *u*-test are shaded, where the yellow and blue are corresponding to positive and negative anomalies respectively. Red contours with 5m/s interval denote the 200-mb zonal wind which are not less than 20m/s. Blue vectors denote the 850-mb wind anomalies (unit: m/s) which are significant at the 99% confidence level of *u*-test. Red arrows denote the preferred transition chain.

positive large-scale rainfall anomalies simultaneously appear over the areas of Northeast China and the MLYRV, which still need further investigations.

(iv) R_4: Yellow River (hereafter YR) regime (Fig. 2(d)). This regime, the same as the Yellow River regime depicted in ref. [17], exhibits a north-south seesaw that significant positive anomalies cover the YR basin with a center located from the middle YR basin to southern Chinese Loess Plateau, and relatively weak negative anomalies region lies on the south of the Yangtze River. Comparatively, the YR regime is almost opposite to the SY regime. Its corresponding anomalous circulation (Fig. 3 C_4), roughly contrary to that of Fig. 3 C_2, is primarily represented by a northwest-southeast "+ – + –" wavetrain in the East Asian areas. Furthermore, the northward and westward positions of the enhanced SHWP are helpful to more northward moisture transport induced by stronger southerlies. Also, both the blockings over the Ural and the northern Pacific, and the significant quasi-annular negative anomalies are considerable.

(v) R_5: Northern regime (Fig. 2 (e)). Many patterns are analogous to Fig. 2 (e) in previous investigations[4,5]. Significant positive anomalies in Fig. 2 (e) appear north of 35°N and in South China with a center in northern North China, and an out-of-phase negative center is located in the Yangtze River valley. The anomalous circulation fields C_5 in Fig. 3, which are by and large opposite to C_1 in Fig. 3, are clearly characterized by the dominant positive center in eastern China areas which shows the extreme northward extension of the SHWP. Furthermore, the positive and negative anomalous centers surrounding the North Pole hint that zonal circulations prevail in mid-high latitude. There exists a south-north "– + –" wavetrain over East Asia, through polar vicinity, reaching to middle North America, which is consistent with the wave train detected by Huang[24] and corresponding to the rainless in the Yangtze River and Huaihe River Basin (YRHRB) and the rainy in the north, due to the stronger Ural blocking and the northward SHWP. Besides, both negative height anomalies over northern India and above-normal westerlies over southern Asia indicate that southwest monsoon flows extending to the eastern China areas are evidently enhanced, which make rainbelt prominent northward.

(vi) R_6: Northwestern regime (Fig. 2(f)). This regime, which is not related in the past literatures on rainfall patterns partially attributed to sparse stations and scarce gauges in Northwest China (NWC), exhibits the significant positive anomalies almost covering the whole of NWC. As seen in C_6 of Fig. 3, its corresponding circulation anomalies are represented by the noticeable wavetrain from west to east along mid-high latitude, the positive centers of which are in turn located in the Caspian Sea-Ural, central-eastern China, and the northwestern Pacific, respectively. Especially, there is a significant negative center of height anomalies where the Xinjiang Ridge often lies, which redounds to the northward water vapor transport from southern oceans to NWC across or round the Qinghai-Tibet Plateau, and then increases precipitation in the region of NWC. In addition, significant negative anomalies exist in the low-latitude Pacific.

(vii) R_7: Yangtze-Huaihe valley (hereafter YH) regime. The positive anomalies in Fig. 2(g) principally extend along the Yangtze River, with the center located between the middle pattern and south pattern[5], and the negative ones exist in eastern NWC. This situation, especially the features of summer rainfall anomalies over the YRHRB, can be seen in many literatures[1−5,10,11]. The circulation anomalies in East Asia (Fig. 3 C_7) are featured by the wavetrain corresponding to the rainy in the YRHRB analyzed by Huang[24], with the stronger blockings over Northeast Asia and the southward SHWP, which indicate a developing meridional circulation pattern. Besides, similar to the SY regime, due to the positive height anomalies in the regions from northern India to the Bay of Bengal and the negative ones in the low-latitude areas, the southwest monsoon flows extending to the eastern China are clearly weakened so that all of the above characteristics of circulation anomalies make the summer monsoon rainbelt southward. The first SVD detected by Lau and Weng[25] represented similar features to Fig. 3C_7, and its coupled anomalous rainfall pattern just is the rainy over the Yangtze River valley.

Thus it can be seen that the seven LFRRs describe the large-scale LFR modes and may be regarded as the improvements on the classifications identified by using stations data[16,17] as the grid data have more homogeneous distributions and the better representations. In fact, we have examined the holistic similarities between different distributions of countrywide rainfall anomalies in terms of carrying out the clustering in phase space and classifying high-correlation samples into the same cluster. On the other hand, as the geographical meanings implied in the RRs' names, a dominant sig-

nificant center exists in every RR, which also gives prominence to the local features of rainfall anomalies. Therefore, when the LFRRs persist and keep their holistic features unchanged, the regional dominant centers are characterized by moving slowly, which is corresponding to the continuous spread[10—13] of LFR, whereas when the transitions between the LFRRs occur, the dominant centers transfer into the other regions, along with which the RRs' holistic features clearly change and the spatial modes of LFR are represented by the abrupt jump.

The composite maps of the LFRRs are reproduced by using unfiltered daily precipitation anomalies of the 160 base stations over China (figures omitted), which reflect consistent features with Fig. 2, except for a few flaws including weaker intensities and reduced significant ranges at the 95% confidence level of positive centers, and obvious disturbances of isograms, as well as diminishing areas of significant negative anomalies. This shows that the spatial interpolation and temporal filtering are reasonable and indispensable to the LFRRs' identification. Furthermore, the low-frequency components in excess of 20-day timescale can depict the principal features of distribution of large-scale rainfall anomalies.

2.3 Climatology of intraseasonal distribution of the LFRRs

Fig. 4 presents the daily climate statistic of the number of each RR occurrence. It can be clearly seen that the climatic distributions of RRs-occurrence periods exhibit evident differences from each other. The appearance of the rainless regime displays most areas of China are in negative phase of LFR oscillation, and is only less from July to the middle ten days of August, when the YH regime appears frequently. The SY regime always occurs before the middle ten days of July, whereas the YR regime and the northern regime often appear in July and after. Towards the eastern regime and the YH regime, as one falls, the other rises. Again, the occurrence of the northwestern regime looks like that of the rainless regime. It can be seen that the intraseasonal distributions of the LFRRs are climatologically featured by large variations, and are corresponding to summer monsoon rainbelts, which shows that LFR plays an important role in total summer rainfall. Consequently, when the mechanism of large-scale rainfall anomalies is investigated, we should keep our eyes on the LFRRs, especially on the features of transitions between them.

3 Features of transitions between the LFRRs

Based on the forementioned analysis on the phase space, it will be quite helpful to reveal the dynamic features of LFR variations by examining the PT relationships between the LFRRs. In other words, the RRs only represent the spacial behavior of LFR anomalies, the alternate transitions between them, however, can comprehensively depict the characteristics of the spatio-temporal variations of summer rainfall anomalies.

3.1 Preferred transitions and circulation backgrounds

Here, a transition is defined as an RR event A ending followed by an RR event B beginning. Certainly, transition may occur between different LFRRs, and the same kind of RR. Table 3 presents the transitions between the RRs during 40 years, forming a Markov transition matrix, where the technique of statistical significance test is the same as that of Mo and Ghil[19].

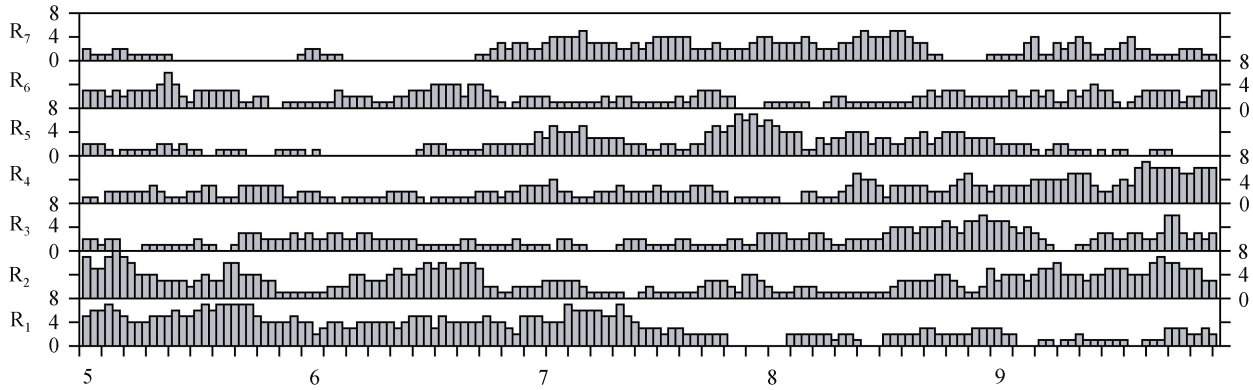

Fig. 4. Accumulated number of daily occurrence of the LFRRs from May to September during 40 years. Unit of ordinate is number of times.

Table 3 Transitions between the LFRRs[a)]

From	To							Sum	Ave. +s.d.	Ave. −s.d.
	R_1	R_2	R_3	R_4	R_5	R_6	R_7			
R_1	4	**13**	**12**	9	4	9	**13**	64	11.94	6.34
R_2	**19**	9	9	7	7	12	7	70	12.93	7.07
R_3	9	4	6	6	6	4	**14**	49	9.45	4.55
R_4	5	6	8	5	**12**	5	7	48	9.28	4.43
R_5	10	5	5	**18**	6	9	1	54	10.29	5.14
R_6	6	**11**	5	**9**	**11**	2	2	46	8.94	4.20
R_7	7	**15**	8	2	6	6	3	47	9.11	4.32
Sum	60	63	53	56	52	47	47	378		

a) Let n be the sum of entries in one row, p=1/7 the equi-probability of transition, including reentry, and q=1–p=6/7. Then the average (ave.) of transitions is np and the standard deviation (s.d.) is $(npq)^{1/2}$; Boldfaces and italics denote significantly likely and unlikely transitions, respectively, determined by taking average + or − s.d. as the significant

It is shown that all of the transitions between the same kind of RR are not significant, and most of them are almost impossible to occur. The PTs are selected in terms of the following criteria: Firstly, selecting the significant transitions including the two inter-transitions ($R_1 \leftrightarrow R_2$ and $R_4 \leftrightarrow R_5$), the seven single-transitions ($R_1 \rightarrow R_3$, $R_1 \rightarrow R_7$, $R_3 \rightarrow R_7$, $R_6 \rightarrow R_4$, $R_6 \rightarrow R_5$, $R_6 \rightarrow R_2$ and $R_7 \rightarrow R_2$); Secondly, selecting the two subsignificant transitions ($R_3 \rightarrow R_1$ and $R_2 \rightarrow R_6$) which mostly appear along with long-lived events. Thus, compared with equi-probability distribution, the PT relationships may be expressed as a PT chain (PTC): $R_1 \leftrightarrow R_3 \rightarrow R_7 \rightarrow R_2 \leftrightarrow R_6 \rightarrow R_5 \leftrightarrow R_4$, where $R_1 \leftrightarrow R_2$, $R_6 \rightarrow R_4$ and $R_1 \rightarrow R_7$ are also included. Of course, this visualized linking is only convenient for analysis and does not mean that the whole PTC must exist (Table 4 and Fig. 5).

As seen in the PTC, the PTs are inclined to occur either between the RRs (R_1, R_3, R_7) with southward positive centers or between the RRs (R_4, R_5, R_6) with northward positive centers, whereas the rainless regime reacts to linkages between the two above situations. For R_1, R_3 and R_7, their anomalous circulation fields are characterized by the south-north "+ – +" wavetrain in East Asia with the stronger SHWP and Northeast-Asia blockings, so the southward PTs may be significantly related to south-north movement of wavetrains over the East Asia-Pacific region (EAPWs). On the other hand, for R_1, R_3 and R_7, their anomalous circulation fields are characterized by the stronger blockings over the Ural, the northern Pacific, and the positive anomalies in eastern China corresponding to the northward SHWP. In the process of $R_6 \rightarrow R_5 \rightarrow R_4$, the linkage between the positive anomalies in Ural and those in eastern China is gradually cut off by the negative anomalies in mid-high latitude over East Asia. The south-north movement of the "– + –" EAPWs has an important effect on $R_5 \leftrightarrow R_4$. Thus it can be seen that the anomalous evolution of the

Table 4 Distributions of the LFRRs, LFRRTMs and conventional RPs (CRPs) from May to September in 40 years[a)]

Year	LFRRs	LFRRTMs	CRPs	Year	LFRRs	LFRRTMs	CRPs
1962	7 1 1 2 **1** 7 2 **1** 3 5 4 **3 7 3** 7 **6**	S, ES	II	1982	3 5 **6 1 2** 7 1 7 **6 1** 6	S	II
1963	3 **4 2** 7 5 3 7 **7** 4 5 **4 3**	ES,N	II	1983	3 6 **4** 4 3 **6** 3 **4**	WN	III
1964	2 5 2 **1 7 5 4** 7 5 4 **5 4** 4 6	S, N	I	1984	4 1 **5 6 3** 3 1 7 6 4	N, ES	II
1965	**2** 1 **2 2 2** 3 3 **7 2** 7 **2** 1	S	II	1985	**4** 2 **3 5 4** 1	N	I
1966	**2 1 4** 5 5 2 **6 2**	S, N, WN	I	1986	2 **6 4 5** 1 3 7 **2** 7 **2**	WN, N, S	III
1967	6 6 5 4 5 **3** 4 4 2 5 **5 4 2**	N	I	1987	**6 4** 7 7 1 **3**	WN, ES	III
1968	2 **1 2 1** 6 **1 7 2** 3 **4** 7 3	S	III	1988	**6 6 4** 5 6 2 4 **1** 3 7 6	WN, N, ES	I
1969	**1 2** 7 3 5 5 **3 7 2 4**	S, ES	III	1989	**2 4** 5 **2 6** 5 4	N, WN	II
1970	1 3 **2 2** 1 2 **1 4** 3 7 2	S, ES	III	1990	4 **3** 5 **6 4** 5 1 **3** 1	WN, N, ES	II
1971	2 3 **3 1 6** 2 **1** 4 3 7	ES, WN, S	II	1991	**2 4** 2 3 7 3 7 **6 3**	ES	II
1972	2 **1** 6 **2** 6 2 4 7 2 **3**	S, WN	II	1992	6 **5** 1 **2** 5 **6 5 4 4** 3	WN, S, WN, N	I
1973	1 3 **1** 3 7 2 **5 4** 4	ES, N	I	1993	**6 1 6** 7 **2** 3 7	WN, S	III
1974	**1** 7 2 3 1 2 **1** 5 **4** 7 3 4	S, N	III	1994	5 **1 1 4 5** 1 5 1 3 **3** 3	S, N	I
1975	**1** 3 1 **4** 5 **4**	ES, N	II	1995	1 2 7 **1** 1 **3 1** 7 6 **5 5** 4 6 4 **5** 6 2 1	ES, N, WN	I
1976	1 3 **1 6 2 1** 5 1 **4**	ES, WN, S, N	I	1996	2 5 **3 7** 1 **6** 5 1 **2 2** 2	ES, WN, S	III
1977	**7** 3 **3 5 5** 4 7 **2** 6 5 6 5 2 **1**	N, S	I	1997	2 **6 3 2 6 1** 2 5 **3 2** 4	WN, S	III
1978	**2 1 2** 2 **5** 2 **3 2**	S, N	I	1998	5 **4** 6 5 6 3 **1 7 5 7 3 6** 2 6 5 6	N, ES, WN	III
1979	1 7 **2** 6 4 **5** 5 **1** 7 1 7 4 6	S, N, S	II	1999	**2 6** 1 6 7 5 **1 1** 4	WN, S	III
1980	**1** 4 3 **4 1** 7 7 **1 7 3 6 2**	S, WN	III	2000	2 6 **2** 7 2 **2**	WN, S	II
1981	2 **1** 4 7 **5** 4 **1 6 4 6** 2	S, N, WN	I	2001	**2 1** 2 4 2 2 2 6 5 **4**	S, N	III

a) The Arabic numerals 1−7 and the Roman numerals I−III denote the seven LFRRs and the three CRPs[5], respectively. Boldfaces denote the events with duration ⩾ 6 days and the preferred transitions are underlined.

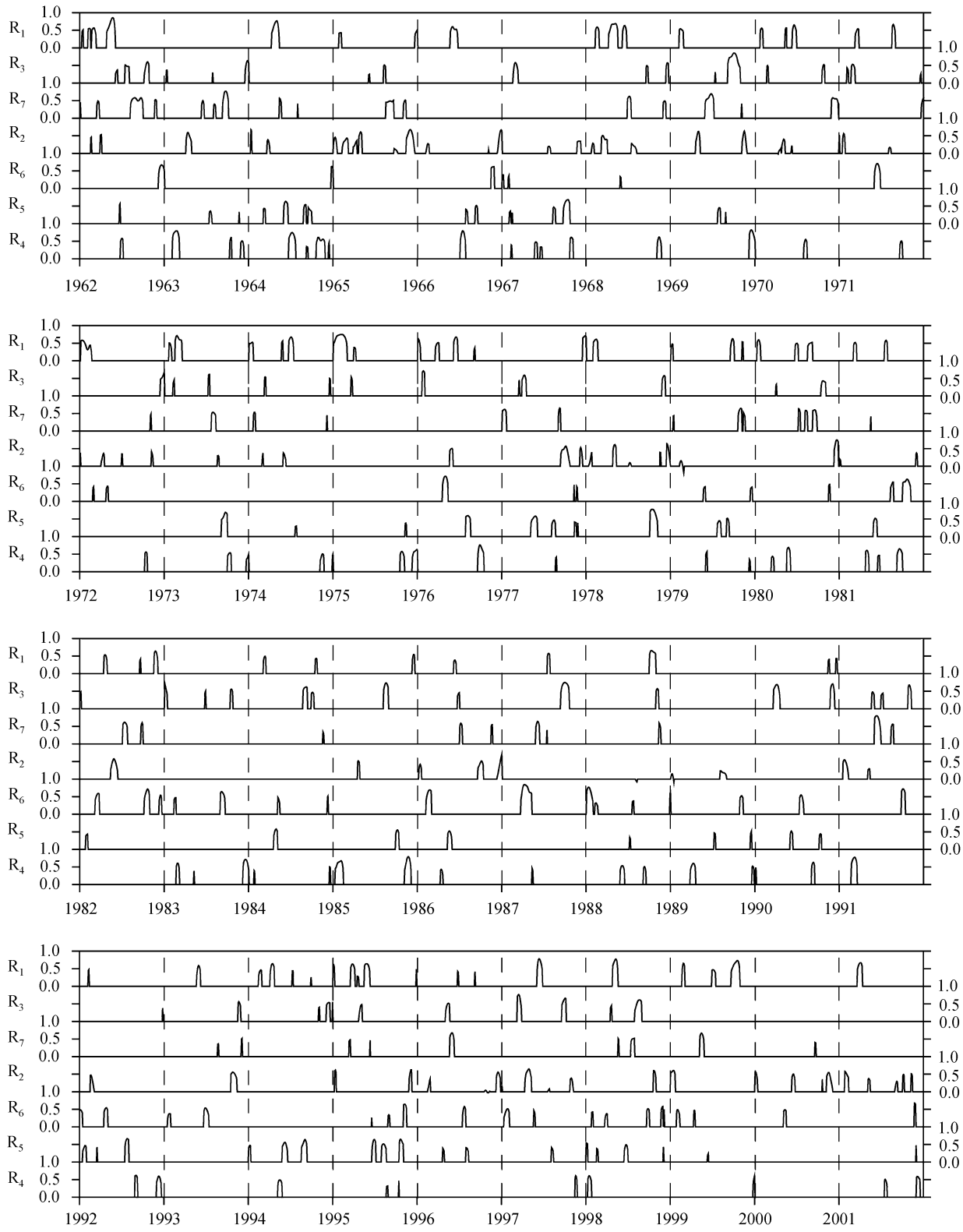

Fig. 5. Correlation coefficients between composite map of each LFRR and its inclusive filtered samples, the period of every year covers from May 1 to September 30 in the abscissa.

SHWP and blockings and the distributions and movements of the EAPWs possibly due to the Rossby wave excitation induced by low-latitude anomalous diabatic heating[24], may be the principal circulation factors of the PTs' existence. Simultaneously, note that diverse groups are likely to exist in the PT relationships owing to the differences of circulation factors.

3.2 Distributions of the LFRRs and PTs in history

Fig. 5 presents the correlation coefficients between the composite map of each RR and its inclusive filtered sample maps (zero is given where no RR appears), which help us visually examine the features of both distributions and transitions of the RRs in history. It can be seen that although only the first 10 EOFs' information is used to the identifications of the RRs, the correlation coefficients in Fig. 5 are still quite high, and nearly all more than the 99% significant level (corresponding correlation coefficient is about 0.23 with 120 degrees of freedom), consequently, which demonstrates that the methods of identifying RRs in the present paper is greatly reasonable. Also, the same correlation analysis has been operated to 500-mb height anomalies (figure omitted), and the correlation coefficients between the composite maps of circulation and their sample maps are still very high, which shows that the relationship between the LFRRs and circulation anomalies is one-to-one, and the same kind of RRs is almost always corresponding to the similar circulation anomalies. On the other hand, height and duration of the "peak" of correlation coefficient curves in Fig. 5, namely the areas covered by the "peak", can effectively reflect the intensity of the RRs. We can see that in a good many years, the intensity of some RRs is so close to each other that it is quite reasonable that the rainfall anomalies of the whole flooding season are described as the combinations of the main LFRRs.

4 LFRRs' transition modes

It is known from the distribution maps of the LFRRs in the 3-dimensional phase space (figure omitted) that the SY regime and YH regime lie in closer positions, which represent the rainy areas in the south; similarly, the northern regime and YR regime represent the north rainy areas; the eastern regime and the northwestern regime represent the rainy areas in the east and the west, respectively. Furthermore, the four inter-transition pairs ($R_1 \leftrightarrow R_2$, $R_4 \leftrightarrow R_5$, $R_1 \leftrightarrow R_3$ and $R_2 \leftrightarrow R_6$) exist in the PTC, which stand for the south, north, east and west primary transitions of the RRs, respectively. Thus, based on the four transition pairs and combined with the analyzed results of the circulation factors of the PTs, the four LFRRs' transition modes (LFRRTMs) are further induced as follows: $R_1 \leftrightarrow R_3$ and $R_3 \rightarrow R_7$ belong to the south mode (S); $R_4 \leftrightarrow R_5$ belong to the north mode (N); $R_1 \leftrightarrow R_3$ and $R_3 \rightarrow R_7$ belong to the northeast-south mode (ES); $R_2 \leftrightarrow R_6$, $R_6 \rightarrow R_4$ and $R_6 \rightarrow R_5$ belong to the northwest-north mode (WN), where only the PTs with the long-lived events ($\geqslant$ 6 days) are utilized. Table 4 gives the distributions of the LFRRs and their transition modes during 40 years, and comparisons with the conventional RPs[5].

It can be found in Table 4 that there exist several RR events in intraseasonal period from May to September, and there occur one or more PTs in every year. The PTs mostly appear between two RRs, and there exist many successive transitions including three, four or even more RRs, for instance, for the years 1973, 1977, 1979, 1986, 1989 and 2001 (Fig. 5). Furthermore, the differences of the LFRRTMs in each year are obvious and the super combinations of one or some LFRRTMs can represent the principal information of LFR in flood season. It should be noted that in some years (1963, 1984, 1993 and 2000), the dominant events, which are not involved in the PTs, are introduced to the PTs by removing the very short long-lived events. For the very especial situations, e.g., R_5 of 1978 and R_1 of 1994 and 1999 are directly regarded as the N and S, respectively. Again, the S and WN, in which the rainless regime is included, often appear in the drought years such as 1972 and 2000.

According to the definition, the LFRRTMs just are the groups of the long-lived events ($\geqslant$ 6 days) in terms of the PTs. Since there exists the good one-to-one relationship between the LFRRs and circulation anomalies, the same kind of LFRRTMs should be also corresponding to the similar circulation backgrounds, which can be seen from the composites of 200-mb zonal wind in Fig. 3. Corresponding to the southward RRs, the jet stream (JS) positions in the C_1, C_3 and C_7 are clearly southward, compared with those of the C_4-C_6 with regard to the northward RRs, which reflects the impacts of the JS position on summer rainbelts[26, 27]. Furthermore, we can also see that the JS axes over East Asia in the C_3 and C_6 are divided into two sections, which is perhaps the direct cause of the eastward and westward RRs, whereas the JS axis in the C_2 related to the rainless regime is obviously eastward in the northwest-

ern Pacific. Consequently, intraseasonal variation of positions and modalities of the East Asian-Pacific jet stream may be principal circulation factors of the four LFRRTMs' formations. Moreover, the JS axes in the C_1, C_3 and C_7 are located above the negative 500-mb height anomalies, however, those in the C_4—C_6 are situated above the positive. Such configurations between the middle and upper circulations may be related to certain anomalous forcing of external heating sources, which is associated with the physical mechanism problem of formations of the LFRRTMs and needs further investigations.

As the interannual and longer scale signals are not eliminated, the super combinations of the LFRRTMs can reflect the information of interannual variability, which may be used to represent the features of the whole summer rainfall anomalies in China. As shown in Table 4, in the years with the same conventional RPs, there actually exists the very different content and it is possible to correspond to the quite distinct atmospheric circulation anomalies and precursory signals. For example, 1998 is an El Niño year, and the regions such as the northeast and northwest China, the mid-low Yellow River valley, and the southern China, are heavily rainy in flooding season, whereas 1999 is a La Niña year and is mainly featured by the rainy over the southern China. Although the two years both belong to the south pattern[8], the circulation situations are obviously different and the LFRRTMs are also quite distinct between the two years. Thus it can be seen that in the years with the same conventional RPs, the circulation anomalies and precursory signals are also possibly quite distinct, but the same LFRRTMs are corresponding to the similar circulation backgrounds, and then are likely to have the similar precursory signals, which still need further to investigate the physical mechanism of the formations of the LFRRTMs.

5 Summary

In the present paper, we have investigated the spatio-temporal features of LFR in summertime over China in phase space. The LFRRs, characterized by persistence and transitions, and the circulation backgrounds of their formations and transitions are examined. The major results of this study have been summarized as follows:

Firstly, a 40-year daily precipitation dataset was produced which includes 200 grid points over most of China from January 1962 to December 2001. In order to extract information of LFR, an EOF analysis was applied to the 20-day low-pass filtered data during the period of summer monsoon from May to September.

Next, in the phase space spanned by the first 10 EOFs, a cluster analysis was used to classify the observed samples and seven LFRRs were identified, namely the SY, rainless, eastern, YR, northern, northwestern, and YH regimes. These LFRRs are corresponding to local extrema of observed probability density in phase space. When a RR appears persistently, the regional dominant centers of LFR are characterized by continuous spread. When transitions between the RRs occur, the spatial modes of LFR are represented by an abrupt jump.

Furthermore, the statistical analyses have shown that the LFRRs are generally consistent with the distribution of summer monsoon rainbelts on the intraseasonal timescale, and there exist PT relationships between them, reflecting the temporal dynamical features of the spatial modes of LFR. In terms of the PT relationships between the RRs, four LFRRTMs have been further induced, which depict the spatio-temporal dual information of the LFRRs and PTs.

The super combinations of the LFRRTMs may be used to represent the features of the whole summer rainfall anomalies in China and are the dominant components of the interannual and intraseasonal variability of summer rainfall. It has followed from the analyses of atmospheric circulation that the anomalies of the SHWP and blockings in mid-high latitude, the low-latitude circulation anomalies, and the EAPWs are significantly related to the persistence and transitions of the LFRRs. Moreover, the anomalous evolution of the SHWP and blockings, and the distribution and movement of the EAPWs, and the intraseasonal variations of positions and modalities of the East Asian-Pacific jet stream may be the principal circulation factors of the formations of the LFRRTMs.

Thus, it is necessary to further investigate the relationships between these circulation factors and anomalous external forcing and the responsible physical mechanisms. Also, it is important to establish a link between the LFRRs including their transition modes and the precursory signals in operational forecasting.

Acknowledgements The authors would like to thank Drs. Yang Song, Li Jianping, Chen Deliang and Shen Xueshun for their valuable comments on the present paper. Thanks are due to the anonymous reviewers for their constructive suggestions to improve the manuscript. This work was jointly sup-

ported by the National Natural Science Foundation of China (Grants Nos. 40135020 and 40375025), and the Ministry of Science and Technology of China (Grant No. 2002ccd00100).

References

1 Deng A J, Tao S Y, Chen L T. EOF analysis of flood-season rainfall in China. Chinese J Atmos Sci (in Chinese), 1989, 13(3): 289－295

2 Tian S F, Yasunari T. Time and space structure of interannual variations in summer rainfall. J Meteor Soc Japan, 1992, 70(1): 585－595

3 Wang X C, Wu G X. Regional characteristics of summer precipitation anomalies over China identified in a spatial uniform network. Acta Meteorologica Sinica (in Chinese), 1996, 54(3): 324－332

4 Wang S W, Ye J L, Gong D Y, et al. Study on the patterns of summer rainfall in eastern China, J of Appl Meteo Sci (in Chinese), 1998, 9(Supplement): 65－74

5 Chen X F, Zhao Z G. Researches on Precipitation Prediction of Flood Season and its Applications in China (in Chinese). Beijing: China Meteorological Press, 2000. 1－241

6 Wang S W. Advance in Modern Climatological Studies (in Chinese). Beijing: China Meteorological Press, 2001. 141－158

7 Chou J F, Xu M. Advancement and prospect of short-term numerical climate prediction. Chin Sci Bull, 2001, 46(18): 1497－1502

8 Zhang P Q, He M, Xu L. Preliminary study on circulation cause of abnormal rich precipitation in and to the south of Yangtze River in summer of 1999. Plateau Meteorology (in Chinese), 2002, 21(3): 243－250

9 Chou J F. Progress of studies on nonlinearity and complexity in atmospheric sciences. Bull Chinese Acad Sci (in Chinese), 1997, 12(5): 325－329

10 Lau K M, Yang G J, Shen S H. Seasonal and intraseasonal climatology of summer monsoon rainfall over East Asia. Monthly Weather Review, 1988, 116(1): 18－37

11 Miao J H, Lau K M. Low frequency oscillation (30-60 day) of summer monsoon rainfall over East Asia. Chinese J Atmos Sci (in Chinese), 1991, 15(5): 65－71

12 Yang G J. The characteristics of low frequency oscillation about rainfall and wind disturbances over eastern China. Chinese J Atmos Sci (in Chinese), 1992, 16(1): 103－110

13 Qian W H, Kang H S, Lee D K. Distribution of seasonal rainfall in the East Asian monsoon region. Theoretical and Applied Climatology, 2002, 73: 151－168

14 Li C Y. Atmospheric Low Frequency Oscillation (in Chinese). Beijing: China Meteorological Press, 1993. 50－83

15 Chen L X, Zhu C W, Wang W, et al. Analysis of the characteristics of 30-60 day low-frequency oscillation over Asia during 1998 SCSMEX. Adv Atmos Sci, 2001, 18(4): 623－638

16 Ren H L, Gao L, Zhang P Q, et al. Primary study on identifying anomalous large-scale rainfall regimes in phase space. Acta Meteorologica Sinica (in Chinese), 2004, 62(4): 459－467

17 Ren H L, Gao L, Zhang P Q, et al. Further study on identifying anomalous large-scale rainfall regimes in phase space. Acta Meteorologica Sinica (in Chinese), 2006, 20(1): 62－71

18 Ghil M, Robertson A W. 'Waves' vs. 'particles' in the atmosphere's phase space: A pathway to long-range forecasting? Proc Natl Acad Sci, 2002, 99(Suppl. 1): 2493－2500

19 Mo K C, Ghil M. Cluster analysis of multiple planetary flow regimes. J Geophys Res, 1988, 93D: 10927－10952

20 Cressman G P. An operational objective analysis system. Monthly Weather Review, 1959, 87(10): 367－374

21 Zhang B L, Chou J F. Applications of EOFs to numerical climatic simulation, Sci China Ser B (in Chinese), 1991, 21(4): 442－448

22 Zhang B L, Chou J F. A study on the stability of the EOF expanded precision. Acta Meteorologica Sinica (in Chinese), 1992, 50(3): 342－345

23 Zhu B Z, Zhang R X, Lin X C. A preliminary study of the Meiyu long-range processes in EOF phase space. Chinese J Atmos Sci (in Chinese), 2001, 25(6): 817－826

24 Huang R H. The East Asia/Pacific pattern teleconnection of summer circulation and climate anomaly in East Asia. Acta Meteorologica Sinica, 1992, 6(1): 25－37

25 Lau K M, Weng H Y. Recurrent teleconnection patterns linking summertime precipitation variability over East Asia and North America. J Meteor Soc Japan, 2002, 80(6): 1309－1324

26 Ding Y H. Summer monsoon rainfalls in China. J Meteor Soc Japan, 1992, 70(1): 397－421

27 Liang X Z, Wang W C. Association between China monsoon rainfall and tropospheric jets. Q J R Met Soc, 1998, 124: 2597－2623